Applied Physics Express

LETTER

Implantation-and etching-free high voltage vertical GaN p–n diodes terminated by plasma-hydrogenated p-GaN: revealing the role of thermal annealing

Applied Physics Express 12, 051015 (2019) LETTER
https://doi.org/10.7567/1882-0786/ab1813

Implantation-and etching-free high voltage vertical GaN p–n diodes terminated by plasma-hydrogenated p-GaN: revealing the role of thermal annealing

Houqiang Fu[1*†], Kai Fu[1†], Hanxiao Liu[2], Shanthan R. Alugubelli[2], Xuanqi Huang[1], Hong Chen[1], Jossue Montes[1], Tsung-Han Yang[1], Chen Yang[1], Jingan Zhou[1], Fernando A. Ponce[2], and Yuji Zhao[1*]

[1]School of Electrical, Computer and Energy Engineering, Arizona State University, Tempe, AZ 85287, United States of America
[2]Department of Physics, Arizona State University, Tempe, AZ 85287, United States of America

*E-mail: houqiang@asu.edu; yuji.zhao@asu.edu
†Authors contributed equally to this work.

Received January 9, 2019; revised March 30, 2019; accepted April 10, 2019; published online May 1, 2019

Low-damage, low-temperature, and easy-to-implement hydrogen-plasma-based termination is attractive for fabricating implantation- and etching-free GaN power p–n diodes. This work investigates in detail the hydrogenation process and unveils the critical role of thermal annealing. A subsequent thermal annealing is key to thermally driving down hydrogen to fully hydrogenate p-GaN to form the termination. The devices showed a specific on-resistance of 0.4 mΩ cm^2 and a breakdown voltage (BV) of ~1.4 kV. They also exhibited improved BV compared with mesa-etched devices. High temperature performance was also investigated. These results can serve as important references for future developments of GaN power electronics. © 2019 The Japan Society of Applied Physics

III-nitrides and their alloys have shown a variety of applications in optoelectronics,[1–3] photonics,[4,5] and electronics.[6,7] Due to GaN's large bandgap, high breakdown electric field (E_b), and large Baliga's figure of merit (BFOM), GaN-based power electronics have recently garnered considerable interests for high voltage, high-power, and efficient power conversion applications.[6] Bulk GaN substrates have been used to homoepitaxially grow high quality GaN epilayers with much reduced defect densities for the fabrication of novel vertical GaN power devices.[7–9] The vertical device geometry can handle larger voltages and currents with smaller chip area and better capability for scaling and thermal management.[10,11] To date vertical GaN-on-GaN p–n diodes have been reported with promising performances such as low specific on-resistances (R_{sp}) and high breakdown voltages (BV).[12–21]

High voltage power diodes often demand termination techniques to mitigate the premature breakdown at the junction edge.[22] Mesa etching is one of the most commonly used methods to terminate and/or isolate high voltage devices. However, this method can induce etching damages, and usually involves etching beveled mesa sidewalls with well-controlled angles or precise mesa steps, and/or designing sophisticated field plates (FP),[19,23] which complicate the device fabrication process, increase the device capacitance, and cause reliability risks. Another popular method is using ion-implantation to form a high-resistivity layer at the device edge by inducing mid-gap and/or compensating defects. After years of development, this method has been widely used in SiC power diodes.[24] However, it is far from mature for GaN devices.[25] In addition, this technique also necessitates a very high temperature postimplantation thermal annealing (e.g., ~1500 °C)[24] to activate implanted atoms. This high temperature can lead to the decomposition of GaN, which is one of most critical hurdles of ion-implantation in GaN. Furthermore, this process is also highly undesirable due to the generation of detrimental defects and surface degradation[23] resulting in unreliable device performance, and increased fabrication costs.

To overcome these challenges, researchers have explored low-temperature, low-damage, and easy-to-implement plasma-based termination/isolation techniques for GaN power diodes. This technique can enable an implantation-free and etching-free fabrication process for high voltage GaN devices. Reference 25 used nitrogen plasma to form a nitridation-based termination since nitridation has passivation effects and can reduce leakage. Reference 26 reported hydrogen (H_2)-plasma-based termination for GaN p–n diodes. The underlying mechanism is that H can easily form very stable Mg–H neutral complexes with Mg acceptors and passivate p-GaN.[27–29] This process is referred to as the hydrogenation of p-GaN, and can effectively passivate p-GaN into high-resistivity GaN, serving as the termination/isolation in devices. This method may also be utilized in GaN transistors[7,8,29–31] for various purposes such as passivation and termination/isolation. In the H_2-plasma-based termination/isolation technique, the plasma treatment is usually followed by a critical thermal annealing process. However, the role of thermal annealing is still not well understood, and its effect on device electrical properties is still unclear. In this work, by studying samples with different treatments and comparing their electrical characteristics, it is revealed that plasma treatment can only deposit H atoms near the p-GaN surface, and thermal annealing is responsible for thermally driving down these atoms to fully hydrogenate p-GaN. With both treatments, we demonstrate a BV of ~1.4 kV, a R_{sp} of 0.4 mΩ cm^2, and a BFOM of ~5.0 GW cm^{-2} in the vertical p–n diodes. In addition, thermal reliability of this technique and comparisons with conventional mesa-etched structures were also investigated.

GaN p–n diode epilayers were homoepitaxially grown on n$^+$-GaN bulk substrates by metalorganic chemical vapor deposition (MOCVD). The growth was initiated with a 1 μm thick n$^+$-GaN buffer layer, followed by a 9 μm unintentionally doped (UID) GaN drift layer and a 0.5 μm p-GaN layer ([Mg] = 10^{19} cm^{-3}), and finished with a thin p$^+$-contact layer. The source materials for Ga and N were trimethylgallium (TMGa) and ammonia (NH_3), respectively. The precursors for n-type and p-type dopants were silane (SiH_4) and bis(cyclopentadienyl)magnesium (Cp_2Mg), respectively. More information about GaN growth by MOCVD can be found elsewhere.[1] High resolution X-ray diffraction was used to characterize the crystal quality of the epilayers using PANalytical X'Pert Pro, where the full width at half maximum (FWHM) were 53 arcsec and 21 arcsec, respectively. According to the estimation method in Ref. 18, the dislocation density of the epilayers was on the order of

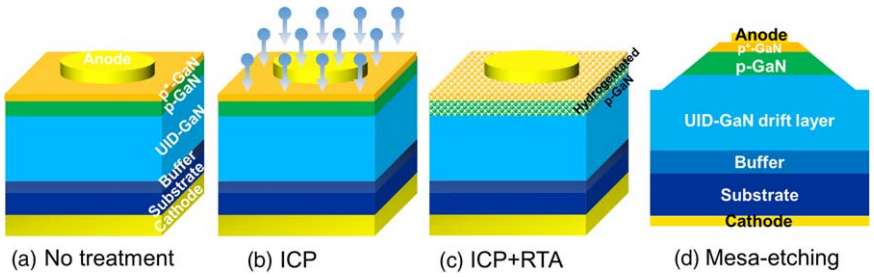

Fig. 1 (Color online) Schematics of samples (a) with no treatment, (b) with ICP treatment, and (c) with ICP and RTA treatments. (d) Schematics of mesa-etched p–n diodes.

$10^6\,\mathrm{cm}^{-2}$. The net carrier concentration N_D of the UID-GaN drift layer was $\sim 5 \times 10^{15}\,\mathrm{cm}^{-3}$ obtained by the capacitance–voltage (C–V) measurement.[32)]

Vertical GaN p–n diodes were fabricated using traditional optical photolithography as shown in Fig. 1. The anode was Pd/Ni/Au metal stacks deposited by electron beam evaporation and subsequently annealed at 450 °C in nitrogen ambient by rapid thermal annealing (RTA). The diameter of the anode is 120 μm. The Ti/Al/Ti/Au cathode were evaporated on the backside of the wafer by electron beam evaporation. To reveal the role of thermal annealing, we performed different treatments on these samples. Some samples had no additional treatments serving as the reference [Fig. 1(a)]. Some samples were subject to H_2 plasma [Fig. 1(b)] generated by STS inductively coupled plasma (ICP) system with an RF power of 10 W and an ICP power of 300 W. The anode can serve as a self-aligned mask where the p-GaN under the anode will not be exposed to the H_2 plasma, and other p-GaN area will be exposed. Some samples with the ICP treatment were further thermally treated by RTA at 400 °C [Fig. 1(c)], which is an optimized temperature. To reduce thermal damages and protect the contacts, the annealing temperature should be minimized. The effectiveness of the thermal annealing on the p-GaN passivation was probed by the currents between two ohmic contacts on the p-GaN after each annealing process. The p-GaN region between the two contacts was exposed to the H_2 plasma treatment. If the exposed p-GaN is fully passivated, there will be no currents flowing between the two contacts. The minimum annealing temperature after which no currents were observed between the two p-GaN ohmic contacts (i.e., reaching the setup limit) was 400 °C. For comparison, mesa-etched devices were also fabricated as shown in Fig. 1(d). The mesa etching with a depth of $\sim$1.5 μm was realized by the chlorine-based ICP dry etching. No passivation or FP were used for all samples. The electrical characteristics of the samples with different treatments were comprehensively analyzed and compared. All electrical measurements were performed on a probe station. The forward and reverse current–voltage (I–V) characteristics were measured by the Keithley 2410 SourceMeter with a high current resolution (voltage limit: 1.1 kV). The breakdown measurements of the devices were carried out by Tektronix 370 A curve tracer with a low current resolution (voltage limit: 2 kV) in Fluorinert electronic liquid FC-70 to prevent flash-over.

Figures 2(a) and 2(b) show the cross-section scanning electron microscopy (SEM) images of samples with different treatments acquired on FEI XL 30 SEM. It should be noted that there are some polishing marks left on the cross-sections due to SEM sample preparations. In addition, the bright contrast on the top surface besides the metal contact in Fig. 2(b) is because the cross-section was imaged at a tilted angle. No difference was observed between the samples with no treatment and with ICP treatment in Fig. 2(a). The exposed p-GaN not covered by the anode did not seem to be affected by the H_2 plasma, showing a similar secondary electron (SE) contrast as the unexposed p-GaN layer [under the anode, to the left of Fig. 2(a)]. However, the sample with the ICP and RTA treatments showed a very different cross-section image. The unexposed p-GaN under the anode remained unaffected, while the exposed p-GaN [outside the anode, to the right of Fig. 2(b)] exhibited a darker SE contrast, similar to the underlying UID-GaN layer, indicating the passivation of Mg acceptors and the hydrogenation of p-GaN. Thus, the hydrogenated p-GaN can provide termination/isolation to the devices to decrease leakage current and increase BV. These results show that ICP treatment alone can only deposit H atoms near the exposed p-GaN surface, and a subsequent RTA treatment is needed to thermally drive down these atoms into the material and fully hydrogenate p-GaN. This mechanism is similar to the thermal diffusion technique used in the doping of semiconductors.[33)] The optical properties of the as-grown and hydrogenated p-GaN were studied using cathodoluminescence (CL) spectroscopy at liquid-helium temperature of 4.6 K. The CL spectra were recorded in raster scan mode using a JEOL 6300 SEM connected to a monochromator and photomultiplier tube. Figure 2(c) shows the CL spectra of as-grown and hydrogenated p-GaN. Two H-related peaks were observed, labeled as DBE1 and DBE2. They have been attributed to H-related deeply-bound excitons (DBE) in p-GaN.[34)] The intensities of DBE1 and DBE2 were largely increased by hydrogenation, indicating that the hydrogenating process created H-related sites in the exposed p-GaN outside the anode. We also observed the donor-acceptor pair (DAP) peak and the neutral acceptor-bound exciton (A_2^0X) peak. The acceptor involved in the A_2^0 X transition is commonly attributed to Mg.[35)] Figure 2(d) shows the Gaussian-fitted CL spectrum of hydrogenated p-GaN at 4.6 K. Seven Gaussian peaks were used to fit the spectrum: A_2^0X at 3.433 eV, DBE1 at 3.386 eV, DBE2 at 3.357 eV, DAP1 at 3.265 eV with its two phonon replicas, and DAP2 at 3.150 eV. The two longitudinal optical (LO) phonon replicas were at 3.173 and 3.081 eV, labeled as LO1 and LO2, respectively. The phonon replicas were restricted to have the same FWHM as their zero phonon line emission. The separation between the phonon lines is 92 meV,

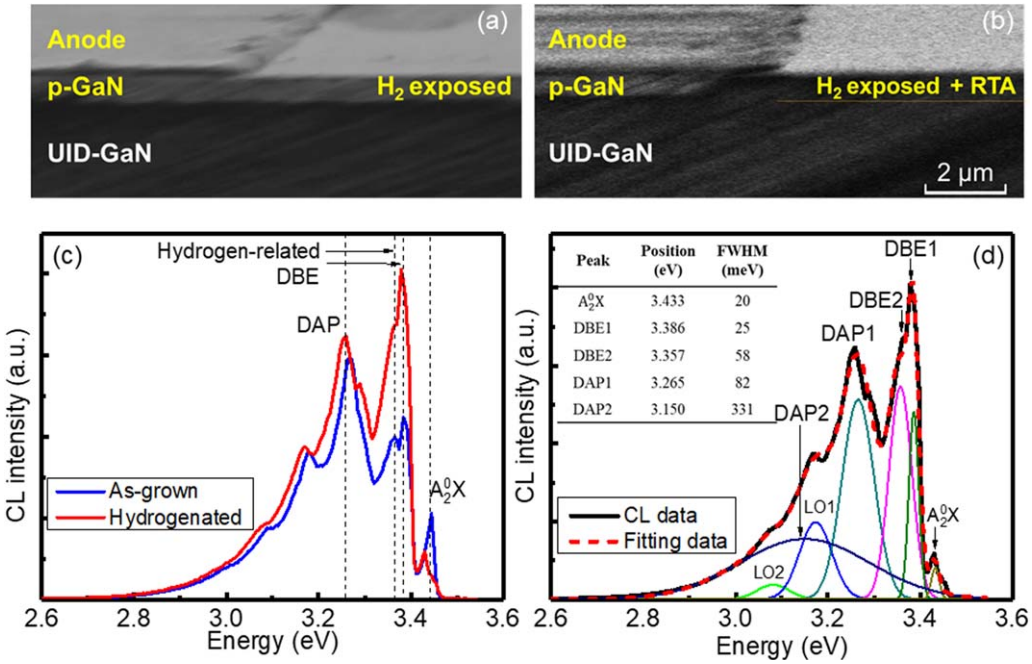

Fig. 2 (Color online) SEM images of samples (a) with no or ICP treatment and (b) with ICP and RTA treatments. (c) CL spectra at 4.6 K of as-grown and hydrogenated p-GaN. (d) Gaussian fitting of CL spectrum at 4.6 K of hydrogenated p-GaN. LO1 and LO2 are phonon replicas to DAP1. The table shows the position and FWHM of the major peaks.

corresponding to the LO phonon energy of GaN. Another DAP transition located near 3.150 eV was observed, labeled as DAP2, and is frequently observed in low-temperature CL of Mg-doped GaN.[34,36)]

To further confirm the proposed role of thermal annealing, the forward and reverse electrical properties of the samples with different treatments were analyzed and compared. Figure 3(a) shows the forward *I–V* characteristics of the three samples in linear and semi-log scales. In linear scale, samples with different treatments showed similar rectifying behaviors with a turn-on voltage (V_{on}) of ~3.4 V. However, in semi-log scale, the sample with no treatment and ICP treatment had much higher leakage current before their turn-on and lower on/off ratio than the sample with ICP and RTA treatments. This indicates that ICP treatment alone cannot form proper termination/isolation for these devices, consistent with the SEM and CL results. In addition, we also observed light emission from these samples, whose spectrum was analyzed by a CCD spectrometer in Fig. 3(b). There were three peaks observed: near-bandgap-edge (NBE)

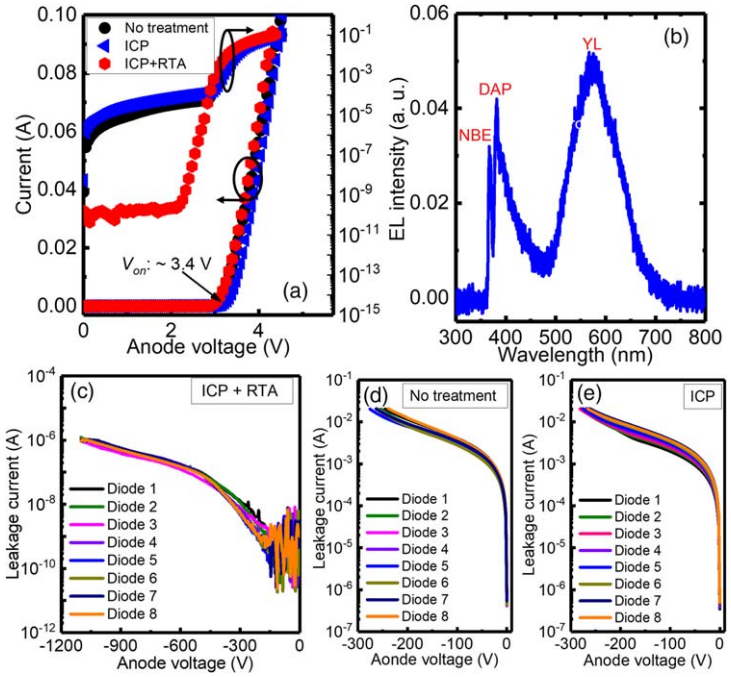

Fig. 3 (Color online) (a) Forward *I–V* characteristics of samples with different treatments in linear and semi-log scales. (b) The EL spectrum of the emission from the device. Reverse *I–V* characteristics of samples (c) with ICP and RTA treatments, (d) with no treatment, and (e) with ICP treatment. Eight representative curves are shown in each treatment.

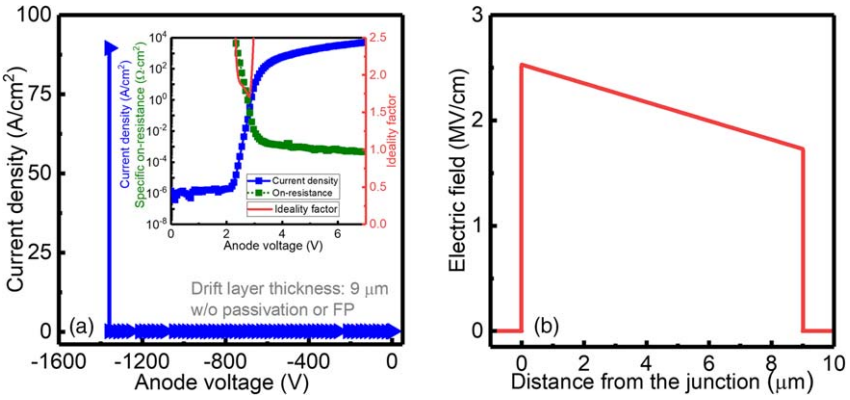

Fig. 4 (Color online) (a) Breakdown measurement of the sample with ICP and RTA treatments. The inset shows the device forward characteristics. (b) The calculated electric field profile inside the device.

emission peak, DAP peak and yellow-luminescence (YL) peak related to the deep-level transition.[37] Figures 3(c)–3(e) compare the reverse leakage currents of the samples with different treatments. The samples with ICP and RTA treatments showed significantly lower reverse leakage current than other samples due to the termination/isolation by the hydrogenated p-GaN. Samples with ICP treatment had a similar leakage current to the sample with no treatment, suggesting the necessity of thermal annealing to the complete hydrogenation of p-GaN for high voltage GaN p–n diodes.

Figure 4(a) demonstrates the reverse breakdown and forward characteristics of the sample with ICP and RTA treatments. Due to the low current resolution of the Tektronix 370 A curve tracer, the breakdown result was plotted in a linear scale. The on-current reached ~5 kA cm^{-2} and the R_{sp} was 0.4 mΩ cm^2. The on/off ratio was ~10^{10}, among the highest values reported in vertical GaN p–n diodes.[15,16,18,38] The ideality factor of diodes can be calculated as a function of voltage by[9]

$$n = \frac{q}{2.3kT}\frac{1}{d\log(J)/dV}, \tag{1}$$

where n is the ideality factor, k is the Boltzmann constant, T is temperature, and J is the current density. The minimum ideality factor was 1.6 at a bias of 2.8 V. Without passivation or FP, the device reached a BV of ~1.4 kV. The breakdown was due to the edge breakdown and resulted in the permanent damage of the device, as visually confirmed by the optical microscopy. The BFOM was calculated to be ~5.0 GW cm^{-2}, which is close to the fundamental limit of GaN. Using the punch-through junction model, the breakdown electric field E_b can be calculated by[19,38]

$$BV = E_b t - \frac{qN_D t^2}{2\varepsilon_0\varepsilon_r}, \tag{2}$$

where t is drift layer thickness. The E_b was estimated to be ~2.5 MV cm^{-1}. Based on Eq. (3),[9] the electric the electric field profile of the device was plotted in Fig. 4(b)

$$dE/dt = -\frac{qN_D}{\varepsilon_0\varepsilon_r}. \tag{3}$$

To investigate the thermal stability of the hydrogenated p-GaN, the I–Vs between two ohmic contacts on p-GaN with the ICP and RTA treatments were measured at different temperatures as shown in Figs. 5(a)–5(b). Compared with the p-GaN, the hydrogenated p-GaN is highly resistive and stable up to 300 °C. The high thermal stability of hydrogen in p-GaN has also been theoretically and experimentally studied by previous reports,[27,39] and it is attributed to the strong bond between H and Mg acceptors in the Mg–H complexes. Figures 5(c)–5(d) present the temperature-dependent forward I–V characteristics of the sample with ICP and RTA treatments. The devices exhibited good rectifying behaviors even at 300 °C. Figure 5(e) shows the extracted V_{on} and R_{sp} as a function of temperature. The V_{on} had a small decremental rate of 1.8 mV °C^{-1}, where the reduction is due to the exponentially increasing diode diffusion current.[19] The R_{sp} slightly increased at a rate of 0.55 μΩ cm^2 °C^{-1} due to the enhanced phonon scattering and thus reduced carrier mobility at high temperatures.[9] Figure 5(f) shows the reverse breakdown measurements at 25 °C and 75 °C. The reverse I–Vs were only measured up to 75 °C due to the strong evaporation of the Fluorinert liquid. Without the Fluorinert liquid, the surface flash-over and surface breakdown will occur, and the real BV of the devices will be underestimated. BV at 75 °C do not show significant degradations compared with those at room temperature.

Figures 6(a)–6(b) compare the forward and reverse I–V characteristics of the sample with ICP and RTA treatments and commonly used mesa-etched p–n diodes. Both devices showed similar forward I–V characteristics. However, the devices with the mesa etching showed considerably smaller BV of ~1 kV and E_b of ~1.8 MV cm^{-1}. Mesa-etched devices usually use additional passivation layers and FPs for high voltage applications, complicating the fabrication process and increasing the costs. In contrast, without etching needed, the plasma-based termination/isolation technique ensures that the junction edge is intact. Figure 6(c) shows the benchmark plot for reported vertical GaN-on-GaN p–n diodes.[12–21] Most of the previous reports[14–17,19–21] involved either thick drift layers (15–40 μm), and/or FPs, and/or high temperature implantation-based termination. Using a relatively thin drift layer of 9 μm, the devices in this work with a simple termination technique achieved high performance close to the GaN limit. This method can vastly simplify the fabrication processes, reduce parasitic effects and reliability issues, and cut down costs for high-power GaN p–n diodes.

In summary, this work studied the role of thermal annealing in the plasma-based termination/isolation technique for the fabrication of implantation- and etching-free

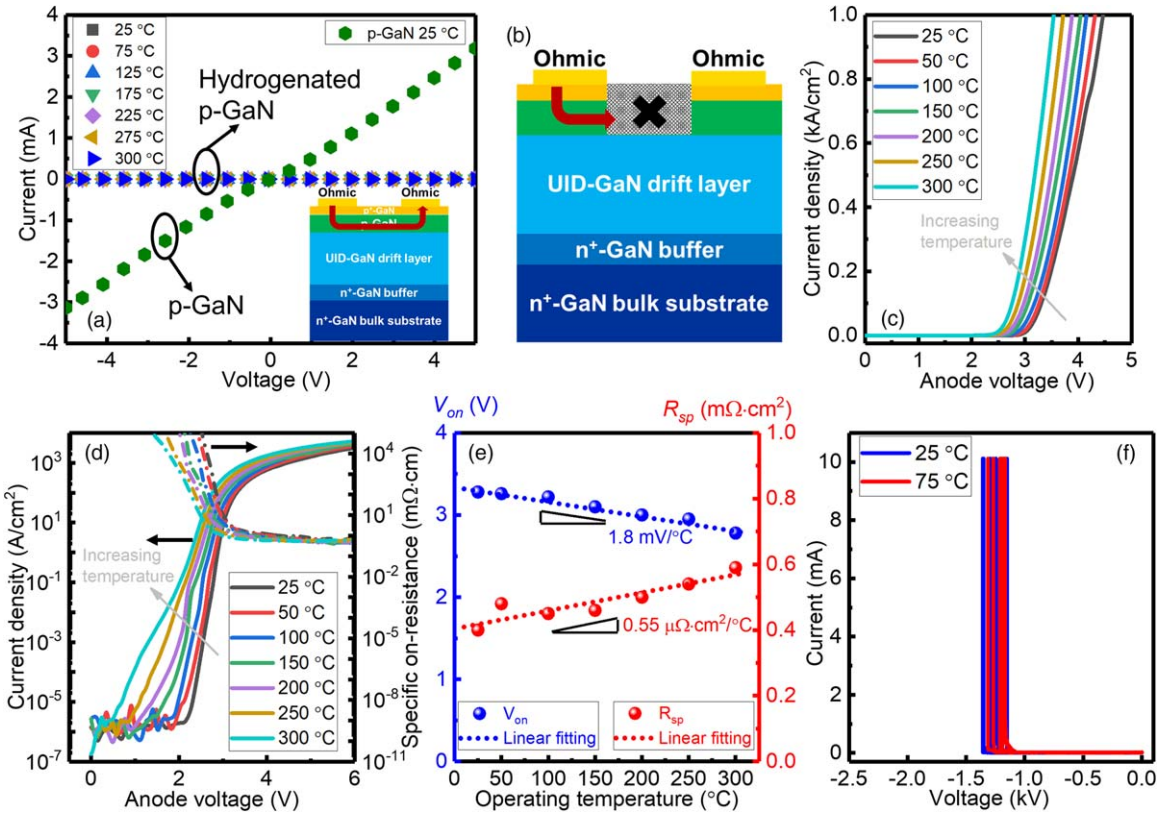

Fig. 5 (Color online) (a) *I–Vs* between two ohmic contacts on p-GaN with the ICP and RTA treatments at different temperatures. The *I–V* between two ohmic contacts on p-GaN is also shown as a comparison. The inset shows the current conduction path in p-GaN. (b) The current conduction path is cut off in hydrogenated p-GaN. Temperature dependent forward *I–V* characteristics of the sample with ICP and RTA treatments from 25 °C to 300 °C in (c) linear scale and (d) semi-log scale. (e) The extracted V_{on} and R_{sp} as a function of temperature. (f) Reverse breakdown *I–Vs* of the sample with the ICP and RTA treatments (eight devices) at 25 °C and 75 °C.

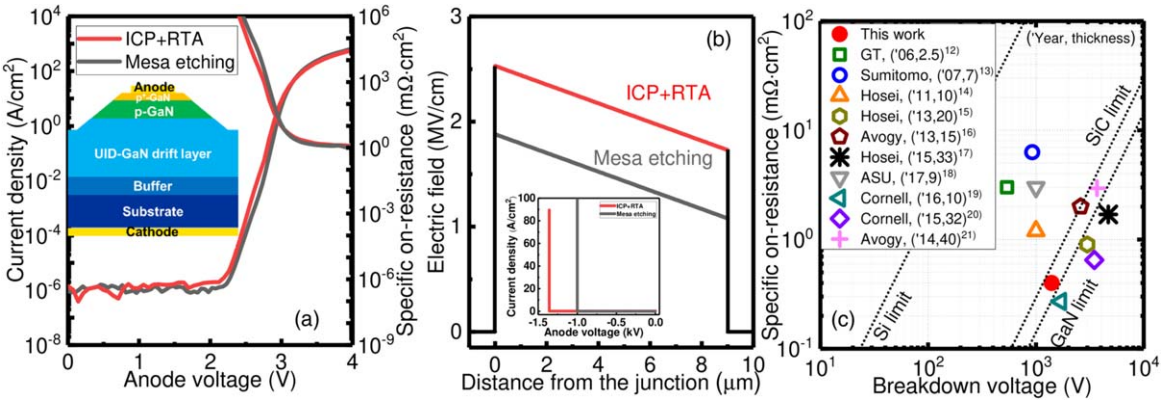

Fig. 6 (Color online) Forward *I–Vs* and R_{sp} for the sample with ICP and RTA treatments and mesa-isolated GaN p–n diodes with the same epitaxial structure. The inset shows the structure schematics of p–n diodes with mesa etching. (b) Electric field profile for the two devices. The inset shows the breakdown measurements of the two devices. (c) Comparison of R_{sp} and *BV* for vertical GaN p–n diodes grown on bulk GaN substrates. All the data are as-reported values in Refs. 12–21, expect that values in Ref. 19 and Ref. 20 are recalculated using the anode area for a direct comparison according to Ref. 40.

vertical GaN p–n diodes. Plasma treatment provides H atoms near the surface, and thermal annealing can drive down these atoms to hydrogenate p-GaN to serve as termination/isolation for the devices. With both plasma and thermal annealing treatments, a *BV* of ~1.4 kV and a R_{sp} of 0.4 mΩ cm^2 were obtained with high on-current, high on/off ratio, and low reverse leakage current. The devices also showed good rectifying behaviors at high temperatures. The *BV* was also largely enhanced compared with the mesa-etched p–n diodes. The simple termination/isolation technique can greatly reduce the fabrication complexity and costs and increase yield and reliability due to low-damage and low-temperature fabrication processes. These results show the great potential of this technique for high voltage and high-power applications.

Acknowledgments This work is supported in part by ARPA-E PNDIODES Program monitored by Dr. Isik Kizilyalli and in part by NASA HOTTech Program grant number 80NSSC17K0768. We acknowledge the use of facilities within the Eyring Materials Center at Arizona State University. The device fabrication was done at the Center for Solid State Electronics Research at Arizona State University. Access to the NanoFab and/or EMC was supported, in part, by NSF award number NNCI-1542160. The samples are provided by IQE

KC, LLC. We thank Prof. Huili Grace Xing from Cornell University for helpful discussions on the device on-resistance.

ORCID iDs Houqiang Fu https://orcid.org/0000-0002-1125-8328 Xuanqi Huang https://orcid.org/0000-0002-7085-4162

1) S. Nakamura, G. Fasol, and S. J. Pearton, *The Blue Laser Diode: The Complete Story* (Springer, Berlin, 2000) 2nd ed.
2) Y. Zhao, H. Fu, G. T. Wang, and S. Nakamura, Adv. Opt. Photonics **10**, 246 (2018).
3) H. Fu, H. Chen, X. Huang, Z. Lu, and Y. Zhao, J. Appl. Phys. **121**, 014501 (2017).
4) H. Sun, Phys. Status Solidi A1800420 (2018).
5) Y. Wang, X. Wang, B. Zhu, Z. Shi, J. Yuan, X. Gao, Y. Liu, X. Sun, D. Li, and H. Amano, Light Sci. Appl. **7**, 83 (2018).
6) S. Chowdhury and U. K. Mishra, IEEE Trans. Electron Devices **60**, 3060 (2013).
7) Y. Zhang, M. Sun, D. Piedra, J. Hu, Z. Liu, Y. Lin, X. Gao, K. Shepard, and T. Palacios, 2017 IEEE Int. Electron Devices Meeting (IEDM), 2017 9.2.1.
8) D. Ji, A. Agarwal, H. Li, W. Li, S. Keller, and S. Chowdhury, IEEE Electron Device Lett. **39**, 863 (2018).
9) H. Fu, X. Huang, H. Chen, Z. Lu, I. Baranowski, and Y. Zhao, Appl. Phys. Lett. **111**, 152102 (2017).
10) Y. Zhang, A. Dadgar, and T. Palacios, J. Phys. D: Appl. Phys. **51**, 273001 (2018).
11) D. Ji and S. Chowdhury, IEEE Trans. Electron Devices **62**, 2571 (2015).
12) J. B. Limb, D. Yoo, J.-H. Ryou, W. Lee, S.-C. Shen, and R. D. Dupuis, Electron. Lett. **42**, 1313 (2006).
13) Y. Yoshizumi, S. Hashimoto, T. Tanade, and M. Kiyama, J. Cryst. Growth **298**, 875 (2007).
14) K. Nomoto, Y. Hatakeyama, H. Katayose, N. Kaneda, T. Mishima, and T. Nakamura, Phys. Status Solidi A **208**, 1535 (2011).
15) Y. Hatakeyama, K. Nomoto, A. Terano, N. Kaneda, T. Tsuchiya, T. Mishima, and T. Nakamura, Jpn. J. Appl. Phys. **52**, 028007 (2013).
16) I. C. Kizilyalli, A. P. Edwards, H. Nie, D. Disney, and D. Bour, IEEE Trans. Electron Devices **60**, 3067 (2013).
17) H. Ohta, N. Kaneda, F. Horikiri, Y. Narita, T. Yoshida, T. Mishima, and T. Nakamura, IEEE Electron Device Lett. **36**, 1180 (2015).
18) H. Fu, X. Huang, H. Chen, Z. Lu, X. Zhang, and Y. Zhao, IEEE Electron Device Lett. **38**, 763 (2017).
19) K. Nomoto, B. Song, Z. Hu, M. Zhu, M. Qi, N. Kaneda, T. Mishima, T. Nakamura, D. Jena, and H. G. Xing, IEEE Electron Device Lett. **37**, 161 (2016).
20) K. Nomoto et al., 2015 IEEE Int. Electron Devices Meeting (IEDM), 2015 9.7.1.
21) I. C. Kizilyalli, A. P. Edwards, H. Nie, D. Bour, T. Prunty, and D. Disney, IEEE Electron Device Lett. **35**, 247 (2014).
22) B. J. Baliga, *Fundamentals of Power Semiconductor Devices* (Springer, Berlin, 2008), Chap. 3.
23) R. Ghandi, B. Buono, M. Domeij, G. Malm, C.-M. Zetterling, and M. Östling, IEEE Electron Device Lett. **30**, 1170 (2009).
24) B. J. Baliga, *Silicon Carbide Power Devices* (World Scientific, Singapore, 2006).
25) S. Han, S. Yang, and K. Sheng, IEEE Electron Device Lett. **39**, 572 (2018).
26) H. Fu, K. Fu, X. Huang, H. Chen, I. Baranowski, T.-H. Yang, J. Montes, and Y. Zhao, IEEE Electron Device Lett. **39**, 1018 (2018).
27) Y. Okamoto, M. Saito, and A. Oshiyama, Jpn. J. Appl. Phys. **35**, L807 (1996).
28) S. Nakamura, N. Iwasa, M. Senoh, and T. Mukai, Jpn. J. Appl. Phys. **31**, 1258 (1992).
29) R. Hao et al., IEEE Trans. Electron Devices **65**, 1314 (2018).
30) C. Gupta, S. H. Chan, Y. Enatsu, A. Agarwal, S. Keller, and U. K. Mishra, IEEE Electron Device Lett. **37**, 1601 (2016).
31) C. Liu, R. A. Khaar, and E. Matioli, IEEE Electron Device Lett. **39**, 74 (2018).
32) H. Fu, I. Baranowski, X. Huang, H. Chen, Z. Lu, J. Montes, X. Zhang, and Y. Zhao, IEEE Electron Device Lett. **38**, 1286 (2017).
33) P. V. Zant, *Microchip Fabrication: A Practical Guide To Semiconductor Processing* (McGraw-Hill, USA, 2004) 5th ed. Chap. 11.
34) R. Juday, A. M. Fischer, Y. Huang, J. Y. Huang, H. J. Kim, J.-H. Ryou, R. D. Dupuis, D. P. Bour, and F. A. Ponce, Appl. Phys. Lett. **103**, 082103 (2013).
35) A. M. Fischer, S. Srinivasan, F. A. Ponce, B. Monemar, F. Bertram, and J. Christen, Appl. Phys. Lett. **93**, 151901 (2008).
36) B. Monemar et al., Phys. Rev. Lett. **102**, 235501 (2009).
37) I. Shalish, L. Kronik, G. Segal, Y. Rosenwaks, Y. Shapira, U. Tisch, and J. Salzman, Phys. Rev. B **59**, 9748 (1999).
38) H. Fu et al., Appl. Phys. Express **11**, 111003 (2018).
39) S. Nakamura, T. Mukai, M. Senoh, and N. Iwasa, Jpn. J. Appl. Phys. **31**, L139 (1992).
40) Z. Hu, K. Nomoto, M. Qi, W. Li, M. Zhu, X. Gao, D. Jena, and H. G. Xing, IEE Electron Device Lett. **38**, 1071 (2017).